COMPDYN 2011
3rd ECCOMAS Thematic Conference on
Computational Methods in Structural Dynamics and Earthquake Engineering
M. Papadrakakis, M. Fragiadakis, V. Plevris (eds.)
Corfu, Greece, 26-28 May 2011

NON-LINEAR DYNAMIC BEHAVIOUR OF A BALL VIBRATION ABSORBER

Jiří Náprstek[1], **Cyril Fischer**[1], **Miroš Pirner**[1] **and Ondřej Fischer**[1]

[1]Institute of Theoretical and Applied Mechanics, v.v.i.
Prosecká 76, Prague 9, Czech Republic.
e-mail: {naprstek,fischerc,pirner,fischero}@itam.cas.cz

Keywords: Vibration ball absorber, Dynamic stability, Nonlinear vibration.

Abstract. *Wind excited vibrations of slender structures such as towers, masts or certain types of bridges can be reduced using passive or active vibration absorbers. If there is available only a limited vertical space to install such a device, a ball type of absorber can be recommended. In general, it is a semi-spherical horizontal dish in which a ball of a smaller diameter is rolling. Ratio of both diameters, mass of the rolling ball, quality of contact surfaces and other parameters should correspond with characteristics of the structure. The ball absorber is modeled as a holonomous system. Using Lagrange equations of the second type, governing non-linear differential system is derived. The solution procedure combines analytical and numerical processes. As the main tool for dynamic stability investigation the 2nd Lyapunov method is used. The function and effectiveness of the absorber identical with those installed at the existing TV towers was examined in the laboratory of the Institute of Theoretical and Applied Mechanics. The response spectrum demonstrates a strongly non-linear character of the absorber. The response amplitudes at the top of a TV tower with ball absorber were reduced to* $15 \div 40\%$ *of their original values.*

1 INTRODUCTION

Passive vibration absorbers of various types are very widely used in civil engineering, especially when wind induced vibration should be suppressed. TV towers, masts and other slender structures exposed to wind excitation are usually equipped by such devices. Conventional passive absorbers are of the pendulum type. Although they are very effective and reliable, they have several disadvantages limiting their application. First of all, they have certain requirements to space, particularly in a vertical direction. These requirements cannot be satisfied any time when an absorber should be installed as a supplementary equipment. Also horizontal construction, like foot bridges, cannot accept any absorber of the pendulum type. Another disadvantage represents a need of a regular maintenance.

Both above shortcomings can be avoided using the absorber of ball type. The basic principle comes out of a rolling movement of a metallic ball of a radius r inside of a metallic rubber coated dish of a radius $R > r$. This system is closed in an airtight case. Such a device is practically maintenance free. Its vertical dimension is relatively very small and can be used also in such cases where a pendulum absorber is inapplicable due to lack of vertical space or difficult maintenance. First papers dealing with the theory and practical aspects of ball absorbers have been published during the last decade, see [1] and [2].

Dynamics of the ball absorber is more complicated in comparison with the pendulum one. Its movement can be hardly described in a linear state although for the first view its behavior is similar to the pendulum absorber type. A number of problems are still open being related with movement stability, bifurcations, auto-parametric resonances and at least but not last with dish and ball surface imperfections. This paper presents basic mathematical model in 2D together with its numerical evaluation and practical application as far as to the state of the realization including some results of long-term measurements.

2 MATHEMATICAL MODEL IN TWO DIMENSIONS

The dish is fixed to a vibrating structure. Their dynamic character is represented by a linear SDOF system represented by a mass M. Inside of a dish an internal ball m in a vertical plane is moving, i.e. 2DOF system should be investigated, as it is outlined in the Fig. 1. It follows from geometric relations:

$$R \cdot \varphi = r(\psi + \varphi) \Rightarrow r\psi = \varrho\varphi \qquad (1)$$

where $\varrho = R - r$. It holds for vertical, or horizontal components of a displacement and velocity of the internal ball centre:

$$\left.\begin{array}{lrcl} \text{horiz.:} & u + \varrho \cdot \sin\varphi & \Rightarrow & \dot{u} + \varrho\dot{\varphi}\cos\varphi \\ \text{vert.:} & \varrho \cdot \cos\varphi & \Rightarrow & -\varrho\dot{\varphi}\sin\varphi \end{array}\right\} \qquad (2)$$

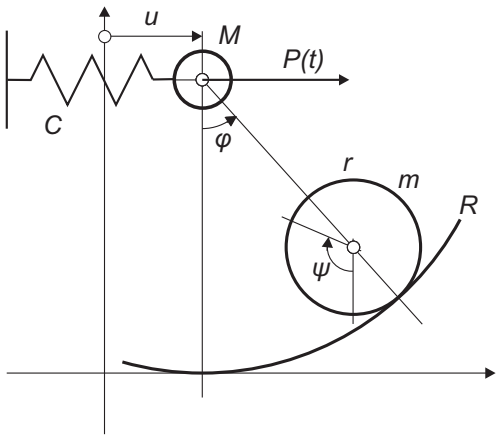

Figure 1: Basic scheme of a system

Kinetic energy of a moving system of balls m, M can be written in a form:

$$T = \frac{1}{2}m[(\dot{u} + \varrho\dot{\varphi}\cos\varphi)^2 + \varrho^2\dot{\varphi}^2\sin^2\varphi] + \frac{1}{2}J\dot{\psi}^2 + \frac{1}{2}M\dot{u}^2 = \frac{1}{2}(m+M)\dot{u}^2 + m\varrho\dot{u}\dot{\varphi}\cos\varphi + \frac{m}{2\kappa}\varrho^2\dot{\varphi}^2 \qquad (3)$$

$m/\kappa = m + J/r^2 \;\Rightarrow\; \kappa = 5/7$, while the potential energy is given by an expression:

$$V = mg\varrho(1-\cos\varphi) + \frac{1}{2}Cu^2 \tag{4}$$

The damping should be introduced in a form of a simple Rayleigh function:

$$B = \frac{1}{2}(Mb_u\dot{u}^2 + mb_\varphi\varrho^2\dot{\varphi}^2) \tag{5}$$

m – mass of the ball m;
J – inertia moment of the ball m;
b_u, b_φ – damping coefficients (logarithmic decrements);

Expressions (3), (4), (5) should be put into the Lagrange equations of the second type, see e.g. [3]:

$$\sum_{r=1}^{n}\left\{\frac{d}{dt}\left(\frac{\partial T}{\partial\dot{q}_r}\right) - \frac{\partial T}{\partial q_r} + \frac{\partial V}{\partial q_r} + \frac{\partial B}{\partial\dot{q}_r}\right\}\delta q_r = P_r(t) \tag{6}$$

$$q_1 = u = \zeta\cdot\varrho\;;\quad q_2 = \varphi\;;\quad P_u(t) = p(t)\cdot M\varrho\;;\quad P_\varphi(t) = 0$$

which give the governing equations of the system:

$$\begin{aligned}
\ddot{\varphi} + \kappa b_\varphi\dot{\varphi} + \kappa\omega_m^2\sin\varphi + \kappa\ddot{\zeta}\cdot\cos\varphi &= 0 \qquad (a)\\
\mu\ddot{\varphi}\cos\varphi - \mu\dot{\varphi}^2\sin\varphi + (1+\mu)\ddot{\zeta} + b_u\dot{\zeta} + \omega_M^2\zeta &= p(t) \qquad (b)\\
\mu = m/M\;;\quad \omega_M^2 = C/M\;;\quad \omega_m^2 = g/\varrho & \qquad (c)
\end{aligned} \tag{7}$$

Eq. (7) describes 2D movement of a ball absorber under excitation by the force $P(t)$ at any arbitrary deviation amplitudes including incidental transition through a limit cycle towards an open regime.

3 THEORETICAL ANALYSIS OF THE ABSORBER

Theoretical efficiency of the absorber will be assessed using its frequency characteristics for excitation of the mass M by harmonic force $p(t) = p_0\cdot\sin\omega t$ simulating influence of external loading or for kinematic excitation of the same mass M. In the later case the movement of the ball m rolling inside of the dish is fully described by Eq. (7a). Should we solve the deviation $\varphi(t)$, Eq. (7b) can serve us subsequently for an evaluation of the force $p(t)$, which is necessary when the deviation $u(t) = \varrho\cdot\zeta(t)$ should be achieved. To obtain frequency characteristics the harmonic excitation $\zeta(t) = \zeta_o\cos(\omega t)$ should be introduced into Eq. (7), which yields:

$$\begin{aligned}
\ddot{\varphi} + \kappa b_\varphi\dot{\varphi} + \kappa\omega_m^2\sin\varphi - \kappa\omega^2\cos\varphi\cdot\zeta_o\cos\omega t &= 0 \qquad (a)\\
\mu\ddot{\varphi}\cos\varphi - \mu\dot{\varphi}^2\sin\varphi + (-(1+\mu)\omega^2 + \omega_M^2)\zeta_o\cos\omega t - b_u\omega\cdot\zeta_o\sin\omega t &= p(t) \qquad (b)
\end{aligned} \tag{8}$$

Eq. (8a). corresponds to the equation of a mathematical pendulum excited in a point of suspension. Its effective mass is increased due to a moment of inertia of the ball m by the factor $1/\kappa = 7/5$. Even in practice the movement amplitudes of this ball do not admit to linearize the Eq. (8a). At least a simple Duffing non-linear form should be retained:

$$\ddot{\varphi} + \kappa b_\varphi\dot{\varphi} + \kappa\omega_m^2(\varphi - \frac{1}{6}\varphi^3) - \kappa\omega^2(1 - \frac{1}{2}\varphi^2)\cdot\zeta_o\cos\omega t = 0 \tag{9}$$

Let us concentrate in this paper to the prior case when the excitation of a harmonic force is taken into account. As the resulting system is auto-parametric, the corresponding methods can be applied, see e.g. [4]. Expecting a single mode response, following approximate expressions for excitation and response can be written (c.f. e.g. [5]):

$$\begin{aligned} p(t) &= p_0 \sin(t\omega) \\ \varphi(t) &= \alpha \sin(t\omega) + \beta \cos(t\omega) \\ \zeta(t) &= \gamma \sin(t\omega) + \delta \cos(t\omega)\} \end{aligned} \tag{10}$$

Having four new variables $\alpha = \alpha(t), \beta = \beta(t), \gamma = \gamma(t), \delta = \delta(t)$ instead of two original unknowns $\varphi(t), \zeta(t)$, two additional conditions can be freely chosen:

$$\dot{\alpha} \sin(t\omega) + \dot{\beta} \cos(t\omega) = 0, \qquad \dot{\gamma} \sin(t\omega) + \dot{\delta} \cos(t\omega) = 0 \tag{11}$$

After substitution (10) and (11) into (7) and substituting the sin and cos functions by two terms of Taylor expansion, the harmonic balance procedure gives differential system for unknown amplitudes $\mathbf{X} = (\alpha, \beta, \gamma, \delta)^T$, see e.g. [6] or [7].

$$\mathbf{M}(\mathbf{X})\dot{\mathbf{X}} = \mathbf{F}(\mathbf{X}) \tag{12}$$

The system (12) for amplitudes $\mathbf{X}(t)$ is meaningful if they are functions of a "slow time", in other words if their changes within one period $2\pi/\omega$ are small or vanishing and individual steps of the harmonic balance operation are acceptable. The matrix $\mathbf{M}$ and right hand side vector $\mathbf{F}$ have the following form

$$\mathbf{M} = \begin{pmatrix} 0 & -\omega & -\frac{1}{4}\alpha\beta\kappa\omega & \frac{1}{8}\kappa\omega A_\alpha \\ \omega & 0 & -\frac{1}{8}\kappa\omega A_\beta & \frac{1}{4}\alpha\beta\kappa\omega \\ -\frac{1}{8}\mu\omega A_\beta & \frac{1}{4}\alpha\beta\mu\omega & (\mu+1)\omega & 0 \\ -\frac{1}{4}\alpha\beta\mu\omega & \frac{1}{8}\mu\omega A_\alpha & 0 & -(\mu+1)\omega \end{pmatrix} \tag{13}$$

$$\mathbf{F} = \frac{1}{48} \begin{pmatrix} 6A_0\kappa\left(3\gamma\omega^2 - \alpha\omega_m^2\right) + 12\omega^2\left(\kappa\left(\alpha\beta\delta + (8-\beta^2)\gamma\right) - 4\alpha\right) - 48\beta\kappa\omega b_\varphi \\ 6A_0\kappa\left(\delta\omega^2 - \beta\omega_m^2\right) + 12\omega^2(\alpha\gamma\kappa + \beta\delta\kappa - 4)\beta + 48\alpha\kappa\omega b_\varphi \\ \omega^2\left(A_0\left(A_0+22\right)\beta\mu - 16(3\delta(\mu+1) - 4\beta\mu)\right) + 48\left(\gamma\omega b_u + \delta\omega_M^2\right) \\ \omega^2\left(A_0\left(A_0+22\right)\alpha\mu - 16(3\gamma(\mu+1) - 4\alpha\mu)\right) - 48\left(\delta\omega b_u - \gamma\omega_M^2 + p_0\right) \end{pmatrix} \tag{14}$$

where

$$A_0 = \alpha^2 + \beta^2 - 8, \;\; A_\alpha = 3\alpha^2 + \beta^2 - 8, \;\; A_\beta = \alpha^2 + 3\beta^2 - 8$$

Determinant of the system matrix $\mathbf{M}$ can be easily evaluated:

$$\det(\mathbf{M}) = -\frac{\omega^4}{4096}\left(64(\kappa-1)\mu + \kappa\mu\Delta_1 R^2 - 64\right)\left(64(\kappa-1)\mu + \kappa\mu\Delta_3 R^2 - 64\right) \tag{15}$$

$$\Delta_1 = \left(R^2 - 16\right), \qquad \Delta_3 = 3\left(3R^2 - 16\right)$$

where $R^2 = R^2(t) = \alpha^2 + \beta^2$ is the amplitude of φ. Polynomial (15) has four roots $R_1^2, \ldots, R_4^2$:

$$3R_1^2 = R_2^2 = 8\left(1 - \frac{\mu+1}{\sqrt{\kappa\mu(\mu+1)}}\right), \; 3R_3^2 = R_4^2 = 8\left(1 + \frac{\mu+1}{\sqrt{\kappa\mu(\mu+1)}}\right) \tag{16}$$

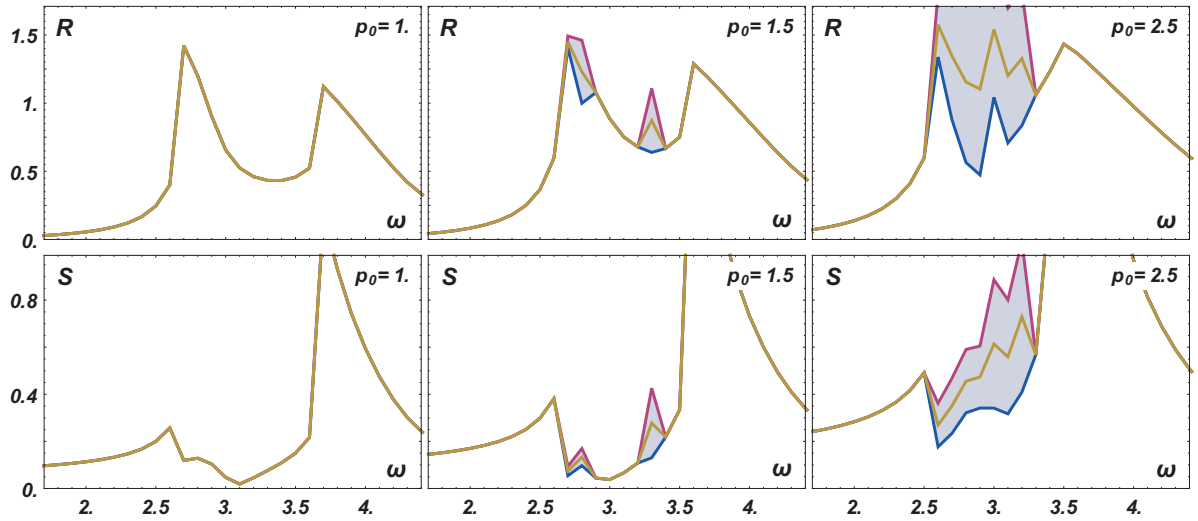

Figure 2: Stabilized numerical solution Eq. (12) . Values of the amplitude $R = \sqrt{\alpha^2 + \beta^2}$ (variable φ, first row) and $S = \sqrt{\gamma^2 + \delta^2}$ (variable ζ, second row) are shown for three selected excitation amplitudes $p_0 = 1, 1.5, 2.5$. The excitation frequency ω is on the horizontal axis. Greyed areas correspond to the frequency region of non-stationary response.

For positive μ and $0 < \kappa < 1$ are the first two roots negative, the last two roots are positive. The negative roots have not any physical meaning, whereas the positive roots form strictly decreasing functions of parameter μ. For $\kappa = 5/7$ (see (3)) it holds:

$$\lim_{\mu\to\infty} R_3^2 = \frac{8}{15}\left(5 + \sqrt{35}\right) \approx 5.82191, \qquad \lim_{\mu\to\infty} R_4^2 = 8\left(1 + \sqrt{\frac{7}{5}}\right) \approx 17.4657 \tag{17}$$

With respect to the meaning of variable φ, even the lower value should not be reached in any real case.

Knowing the exact form and regularity properties of the system matrix $\mathbf{M}$, its inverse could be easily derived and then the normal form of the differential equation (12) can be established. However, as long as the matrix $\mathbf{M}$ is regular, the original right hand side $\mathbf{F}$ can be studied equivalently.

Let us consider stationary response of the system. In this case, the derivatives $\mathrm{d}\mathbf{X}/\mathrm{d}t$ vanish and the right hand side $\mathbf{M}$ has to vanish too. Eq. (12) degenerates to the form of:

$$\mathbf{F}(\mathbf{X}) = 0 \tag{18}$$

Thus, to identify the stationary solutions, the zero solution points of $\mathbf{F}$, depending on the excitation frequency and amplitude, should be traced. In the same time, the signum and the zero points of the Jacobian $\det(\mathbf{JF})$ have to be checked. Negative value of the Jacobian for a particular point indicates that the corresponding solution is stable, whereas when Jacobian vanishes a bifurcation could occur.

The curve $\mathbf{F}(\alpha, \beta, \gamma, \delta, \omega) = 0$, projected into the planes (ω, R) or (ω, S) (for $S^2 = \gamma^2 + \delta^2$), forms the resonance curves known from the analysis of linear oscillators. However, correspondence of this curve to the original equation (7) is limited to the case of stationary response. It is necessary to remind, that limits of stationarity of the response cannot be determined from properties of Eq. (18) itself. The complete Eq. (12) has to be take into account for this purpose.

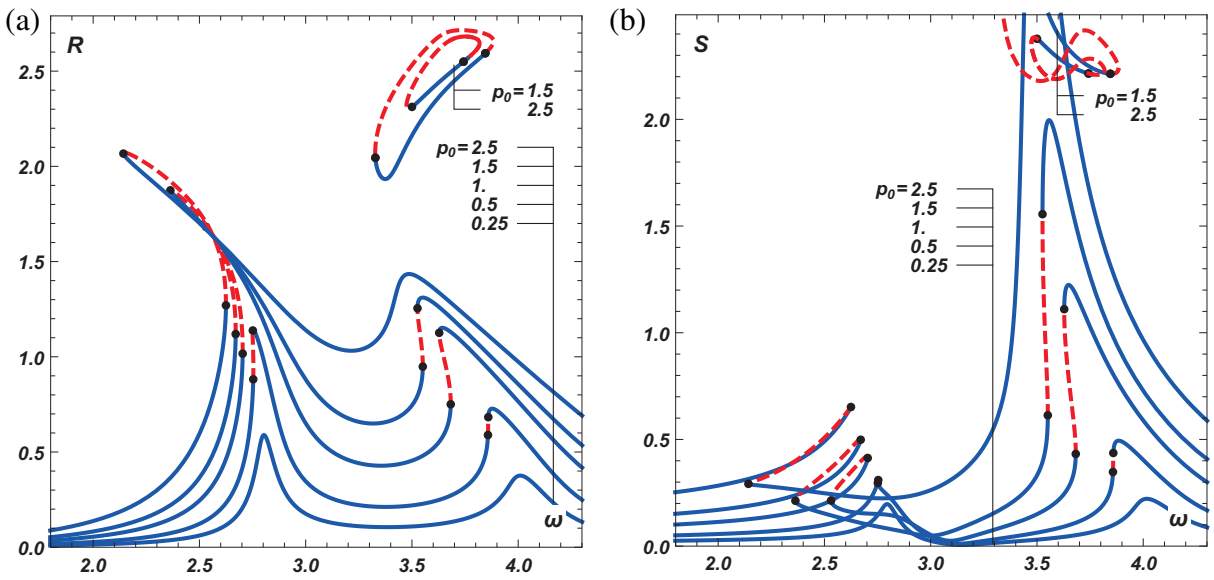

Figure 3: Non-linear resonance curves describing the stationary response of the system computed as zero solutions of Eq. (18) for excitation amplitudes $p_0 = 0.25, 0.5, 1, 1.5, 2.5$. Stable branches are shown as solid blue curves, unstable parts are indicated as the red dashed curves. Amplitudes $R = \sqrt{\alpha^2 + \beta^2}$ are shown in the left part of the figure, amplitudes $S = \sqrt{\gamma^2 + \delta^2}$ are on the right.

4 NUMERICAL ANALYSIS

The aim of this study is a basic engineering approach demonstrating the problem as a whole from the theoretical background until realization in practice. Thus, the numerical analysis has been selected as it leads the most quickly to a basic overview about dynamic properties of a ball absorber.

With respect to actual experiences regarding passive vibration absorbers and some interesting properties of the system (7), following reference input data have been introduced:

$$M = 10.0\ ;\ m = 2.0\ ;\ \varrho = 0.71\ ;\ b_\varphi = 0.1\ ;\ b_u = 0.2\ ; C = 140\ ;\ p_o = 0.5 \div 2.5 \qquad (19)$$

Several analysis procedures have been performed:
(a) Numerical integration of Eq. (7) shows the response characteristics of the system.
(b) Numerical solution of Eq. (12) can help to decide if the response is stable or unstable.
(c) Analysis of the term $\mathbf{F}(\mathbf{X})$ given by Eq. (18) gives the resonance curve including the unstable branches.

Frequency response characteristics of the Eq. (12) for the particular data is shown in the Fig. 2. This non-linear equation has to be solved numerically. Starting from non-trivial initial conditions solution $\alpha(t), \beta(t), \gamma(t), \delta(t)$ stabilizes after certain time. Mean value and standard deviation of the stabilized amplitudes $R = \sqrt{\alpha^2 + \beta^2}$ (variable φ, first row) and $S = \sqrt{\gamma^2 + \delta^2}$ (variable ζ, second row) depending on the excitation frequency ω are shown in Fig. 2. The variance of the amplitudes is shown as greyed area around the mean curve. Thus, the greyed areas indicate regions where a non-stationary solution should be expected (amplitudes R and S are not constant). It should be emphasized here, that validity of the Eq. (12) in non-stationary case is limited, as it was derived with an assumption of slow time change of the amplitudes.

Utilizing the Eqs. (18) and (14), the non-linear resonance curves describing the stationary response of the system (7) can be obtained. A set of such curves for excitation amplitudes $p_0 = 0.25, 0.5, 1, 1.5, 2.5$ is shown in the Fig. 3. It is obvious for the first view the non-linear

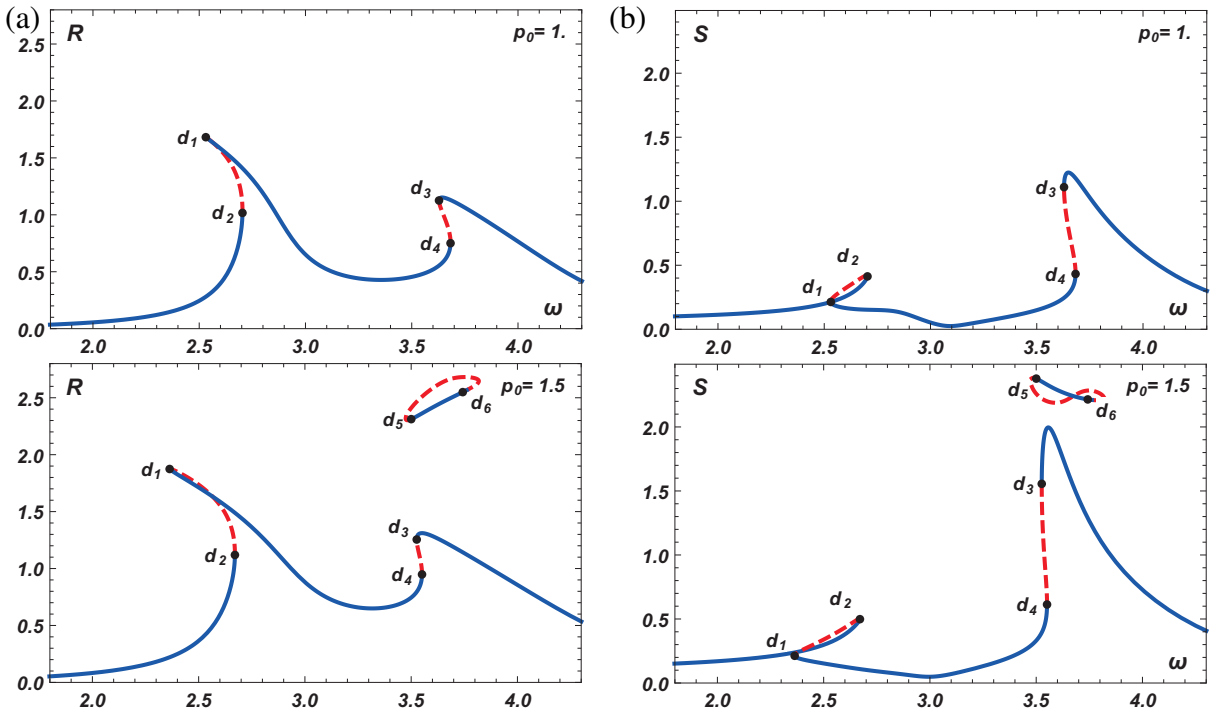

Figure 4: Selected non-linear resonance curve for $p_0 = 1$ and $p_0 = 1.5$. (a) The case for $R = \sqrt{\alpha^2 + \beta^2}$ is on the left, (b) case for $S = \sqrt{\gamma^2 + \delta^2}$ is in the right part of the figure. Points $d_1, ..., d_6$ correspond to zero points of Jacobian $\mathbf{JF}$ and indicate change of stability properties of the curve.

character manifesting oneself by a dependence of a position of extreme points on an amplitude of excitation force. This effect is visible predominantly in a neighbourhood of a conventional "linear" natural frequency of the absorber although also the second natural frequency corresponding to the original natural frequency of the structure is affected. The resonance curves are typical for a system with "softening" non-linearities. It turns out that the non-linear element represented by a ball absorber can be more effective when broad band random response should be reduced. Even better results can be expected in case of non-stationary excitation when amplitude spectrum is significantly variable in time. In such a case no doubt non-linear absorber should be preferred, while the linear one works better in cases of strong narrow band excitation mostly of deterministic character.

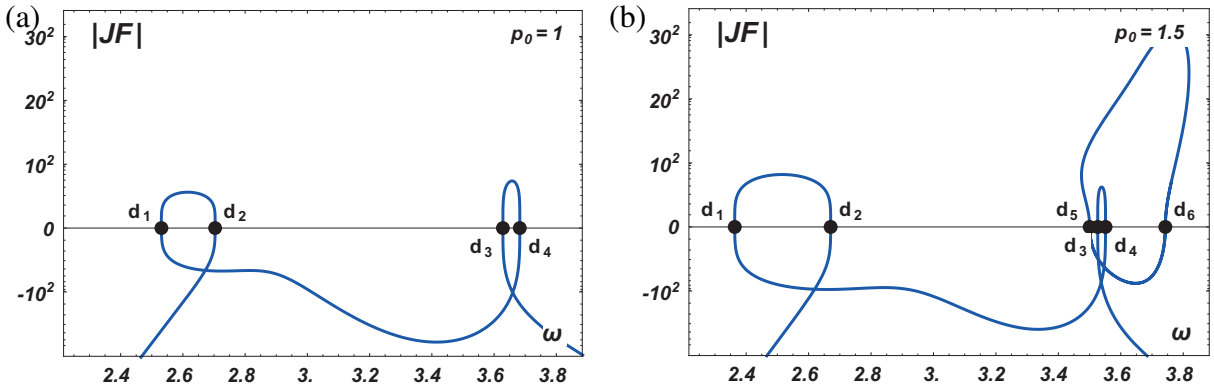

Figure 5: Values of Jacobi determinant $\det(\mathbf{JF})$ corresponding to the stationary resonance curve for $p_0 = 1$ (a) and $p_0 = 1.5$ (b). Negative values indicate stable branches of the resonance curve and vice versa. Closed curve in the right part of fig. (b) correspond to the isolated part of the resonance curve, c.f. second row of Fig. 4.

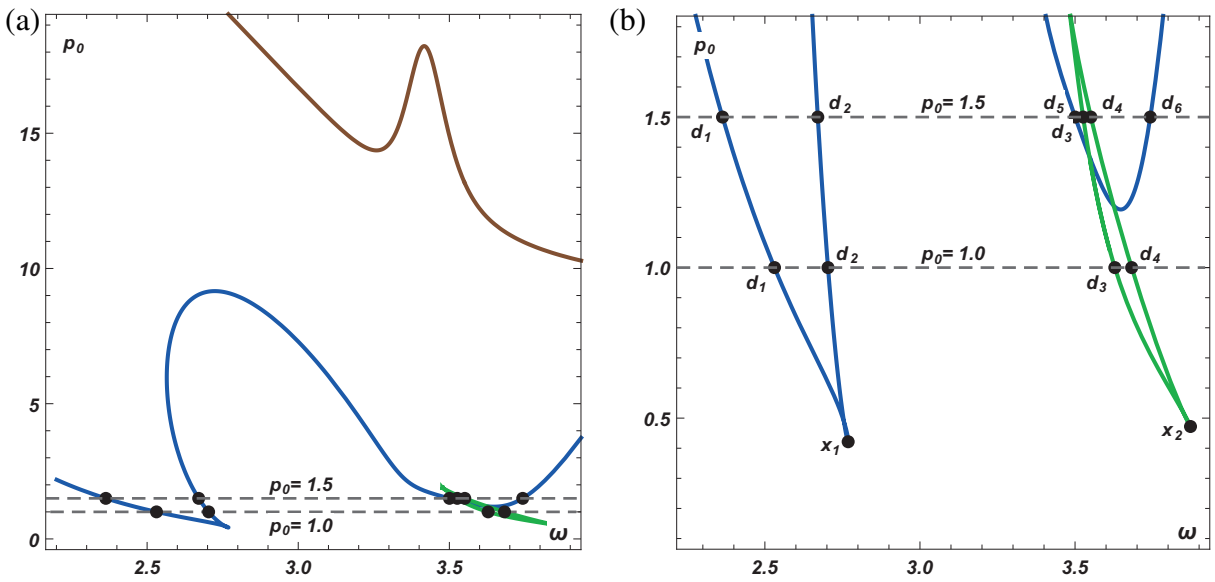

Figure 6: (a) Position of zeroes of the Jacobian in the (ω, p_0) plane. (b) Zoomed view of the interesting area for $p_0 \in (0, 2)$ of the figure (a). Points $d_1, ..., d_6$ are indicated on the level of $p_0 = 1$ and $p_0 = b$, c.f. figures 4 and 5. Points x_1 and x_2 show the critical values of p_0 computed using Eq. (20-21).

Let us comment the isolated curves indicating high amplitudes of response for $p_0 = 2$ and 3. Limit value for R, as it results from the roots of the $\det(\mathbf{M})$ (Eq. (15)) is for data (19) $R < 3.22$. This limit is for the high curves in Fig. 3 still not violated. However, these curves have not any physical meaning in this case: (i) such high amplitudes of R are unrealistic, (ii) Eq. (12) was derived utilizing two terms of Taylor expansions for sin and cos functions and thus assuming only "small" amplitudes.

Let us study in more detail the stability of one particular curve from Fig. 3, the one for $p_0 = 1$. The both R and S (or φ and ζ respectively) resonance dependencies are shown in the first row of Fig. 4. The solid parts of the curves correspond to the stable solution, whereas the red dashed sections correspond to the unstable solution of Eq. (18). Second row of Fig. 4 shows similar curves for higher excitation amplitude $p_0 = 1$. The islolated part of the response curve is present in this case.

Response of a real system cannot be expected to reach values of a unstable part of resonance curve. The stability of the individual sections of the curves follows from the sign of the Jacobian. Course of this value, corresponding to the curves in Fig. 4 is shown in Fig. 5a for $p_0 = 1$ and in Fig. 5b for $p_0 = 1.5$. Here the points $d_1, ..., d_4$ or $d_1, ..., d_6$ correspond to zero points of Jacobian $\mathbf{JF}$ and indicate change of stability properties of the curve, c.f. all parts of Fig. 4. Closed curve in the right part of Fig.5b correspond to the isolated part of the resonance curve.

Existence of the unstable branches could serve as a characteristic of the system from the engineering point of view. It can be stated, that until the system properties (structural parameters) and the expected excitation amplitude are such that no unstable part of the resonance curve occurs, almost linear and stationary behaviour of the system can be expected. Positions of the dangerous values of the excitation amplitude p_0 depending on the excitation frequency are shown in Fig. 6. The overall situation for the system defined by values (19) is shown in the left part of the figure (a), whereas the part of realistic expected amplitudes is shown in the part (b). Positions of points $d_1, ..., d_4$ corresponding to the excitation amplitude $p_0 = 1$ and $d_1, ..., d_6$ for $p_0 = 1.5$ are shown in the both parts of the Fig. 6.

The curves from the Fig. 6 can be relatively easily computed from the algebraic system

$$\begin{aligned} \det(\mathbf{JF}(\mathbf{X},\omega) &= 0 \\ \mathbf{F}(\mathbf{X},\omega,p_0) &= 0 \end{aligned} \tag{20}$$

Having a solution of (20) for any particular value of ω and p_0 the curves can be considered as parameter dependent $\omega(s)$ and $p_0(s)$ and traced e.g. using the arc-length method. The extremal values are then such points $(\omega(s), p_0(s))$ that

$$\partial_s \omega(s_0) = \partial_s p_0(s_0) = 0 \tag{21}$$

To cover all the extremes, the relation (21) has to be used for all interesting solutions obtained from the system (20). For data defined by (19) are the critical values of the amplitude p_0 shown in the Fig. 6 as points x_1 and x_2. Corresponding critical values of p_0 are $p_{0,x_1} = 0.421$ and $p_{0,x_2} = 0.472$ for $\omega_{x_1} = 2.77$ and $\omega_{x_2} = 3.87$.

For sake of comparison, the non-linear resonance curve for $p_0 = 1$ is shown together with result of the frequency response relation, which has been obtained using numerical integration of the original system (7) for excitation amplitude $p_0 = 1$. As it can be seen from the Fig. 7, the agreement is rather good. Relatively low non-stationarity can be seen as the greyed areas of the curve for ω just above points d_2 and d_4. For other excitation amplitudes the graphs resemble the Fig. 3 and thus are not shown here.

It appears, that increasing the excitation amplitude over a certain limit a domain of unstable chaotic response to deterministic excitation emerges. It does not reveal that this domain increases significantly when random instead of deterministic excitation is applied. Nevertheless a presence of chaotic response domain is for the sake of the structure, as the effective response amplitudes are decreasing under these circumstances due to the rapid increase of the entropy of the response probability density.

On the other hand it is necessary to remain realistic. During testing in laboratory many effects corresponding to various critical and post-critical effects have been observed which are not yet described and quantified theoretically.

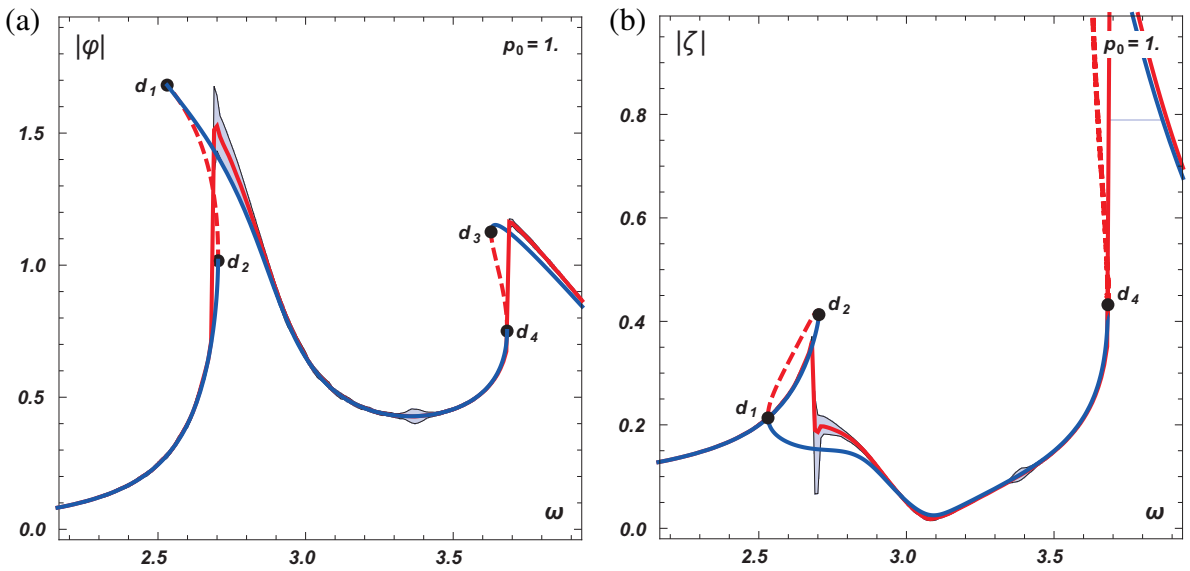

Figure 7: Example of correspondence between stationary resonance curves computed using (14) (blue curves) and response characteristics obtained via numerical integration of Eq. (7) (show in red). Absolute values of the maximum, minimum and mean peak responses of φ are shown on the left and for ζ on the right. Greyed area between minima and maxima curves shows the regions of non-stationary response.

5 APPLICATION OF BASIC THEORY AND EXPERIMENT

First of all two practical knowledge resulting from laboratory experiments and in situ measurements should be mentioned.

As regards the damping, the use of the logarithmic decrement as the measure of damping does not correspond very well to the non-linear nature of the phenomenon. However, a comparison of the behaviour of different physical models which were examined is very useful. Fig. 8 shows the value of the logarithmic decrement b_φ of the model plotted against the absorber - mass ratio μ, see Eq. (7c). The model was put into vibration by initial deflection from its equilibrium position. In this figure diagrams for several values of initial displacement have been plotted. It can be seen that the model without ball ($\mu = 0$) has the damping nearly 0.02 (the point on the horizontal axis $\mu = 0$), while adding ball the damping reaches 0.17-0.25 (the points on the horizontal axis $\mu = 0.2$, curves valid for simple motion) i.e. nearly 8 times more. Similar effect appears also on conventional pendulum absorbers. For details, see [1].

The influence of inclination was also tested on the model, involving the case when the dish of the absorber exercises the rotation about the horizontal axis, coupled with its horizontal translation. The most unfavourable case was tested, i.e. when the frequency of dish inclination approaches the natural frequency of the ball rolling inside the dish (ω_m). No unfavourable increase of the amplitudes of the ball was observed.

The function and effectiveness of vibration ball absorber was described in detail in [2]. Now we shall describe the experiments made in the laboratory. The dish was fastened to a table supported by nine steel balls enabling the excitation of its movement by one, possibly two mutually perpendicular forces. The forces were supplied by one (uniaxial excitation) or two (biaxial excitation) MTS cylinders (jacks) via arms. The "position control" regime was selected in which the excited movement displacement was constant within a frequency range $\omega \in (4.40 \div 9.40 s^{-1})$. Excitation force amplitude was variable being a function of excitation frequency. Two series of experiments have been done. The first one with the internal side of the dish with rubber covering layer and the second one without this covering.

During the excitation by one harmonic force, the excitation frequency was varied within the range $\omega \in (4.40 \div 9.40 s^{-1})$ in steps of $\Delta\omega = 0.5$, and in the resonance domain in steps of

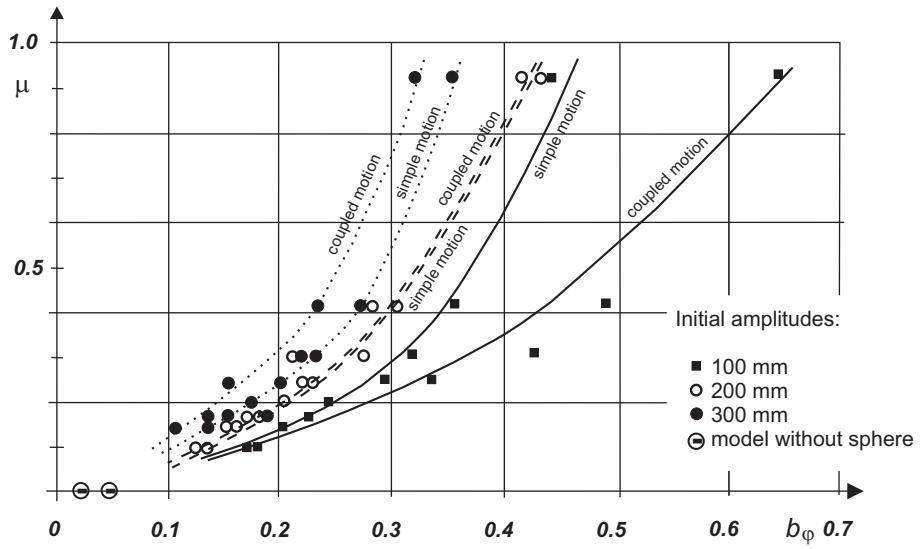

Figure 8: Logarithmic decrement b_φ plotted against the mass-ratio μ for different initial amplitudes

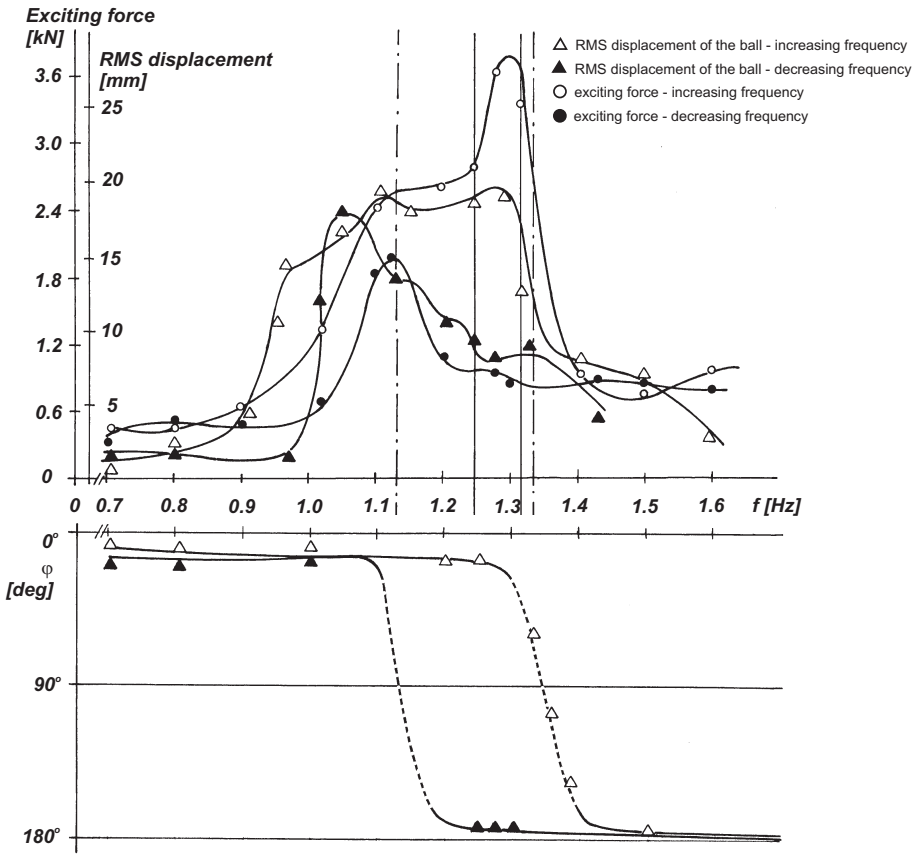

Figure 9: Experimental resonance curves of exciting force and of ball m response

$\Delta\omega = 0.25$. The duration of one step was 30 seconds, the transition from one step to another 15 seconds. Seven amplitudes of table displacements ranging from $1mm$ to $7mm$ were applied. As an example (table displacement amplitude $u_o = 4mm$), Fig. 9 shows the resonance curves of the ball m and dish movement depending on frequency of the excitation force, when the dish is without rubber coating (another plot applies for the state with coating). Fig. 9 shows also the phase shift of the ball and the dish displacement in the excitation direction, once again for the increasing as well as decreasing excitation frequency, see the bottom part in the Fig. 9. Two jumps of phase shift (increase or decrease) within the range $(0 - 2\pi)$ can be observed in a neighborhood of the frequency corresponding with the biggest excitation force values.

The ball, although subjected to uniaxial excitation, performed a movement which comprised also a component deviating from the direction of excitation. This complex 3D ball movement appeared in the dish without rubber lining. The response spectrum contains peaks different from excitation frequency, particularly outside the resonance domain and corresponding rather with multiples of the natural frequency of the linearized system. It is another evidence of significant non-linear character of the system, which manifests this time by super-harmonics of the response.

Relation of logarithmic decrement of the damping and the amplitude $\varphi_o \cdot \varrho$ of the dish is presented in the Fig.10a,b, while the relationship of the natural frequency of the ball (moving on steel and on rubber coating respectively) on the amplitude $\varphi_o \cdot \varrho$ has been outlined in the Fig. 10c.

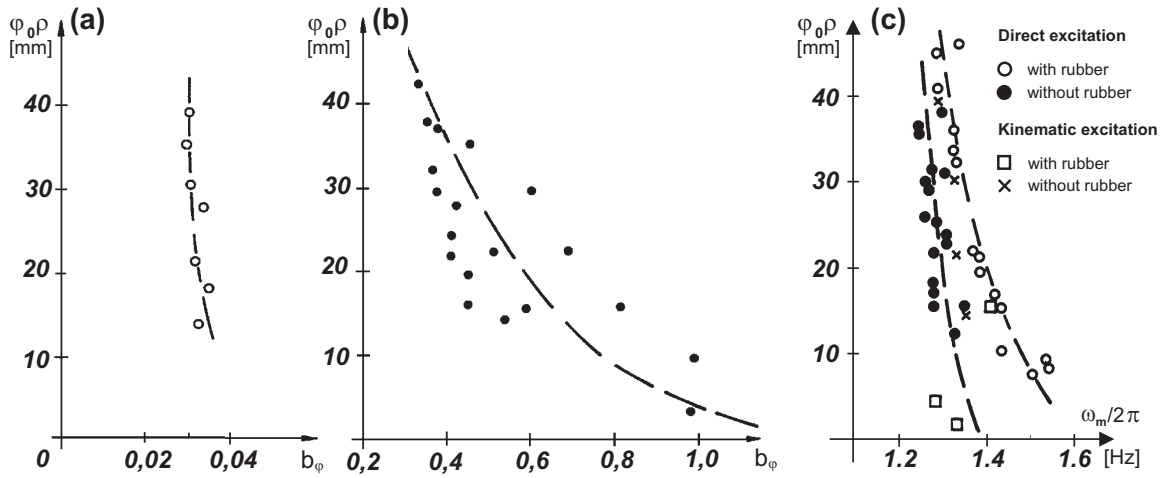

Figure 10: (a) and (b): Relation of logarithmic decrement b_φ and amplitude $\varphi_o \cdot \varrho$ of the ball m,
(c) Relation of natural frequency ω_φ and amplitude $\varphi_o \cdot \varrho$ of the ball m

6 PRACTICAL REALIZATION

The ball absorber was used recently on two TV towers in the Czech Republic to suppress wind excited vibration (Figs 11a, 11b) . Both towers under observation showed two dominant natural frequencies before absorber has been installed $\omega_{(1)} = 7.98s^{-1}, \omega_{(2)} = 10.68s^{-1}$ (nearly identical for both towers). Corresponding natural modes and the amplitude of vibration in wind of mean velocity $8 - 15m/s$ are plotted in the Fig. 11c. The response amplitude at the top of the tower is $10.65mm$, while that at the RC platform level $0.273mm$. Four legs of the steel lattice part were recently strengthened.

The ball absorber before the mounting on the top of the tower presents the photo at the Fig. 12. The most important numerical results demonstrating the absorber efficiency in dimensionless values are outlined in the Tab. 1. The efficiency has been evaluated for the most important

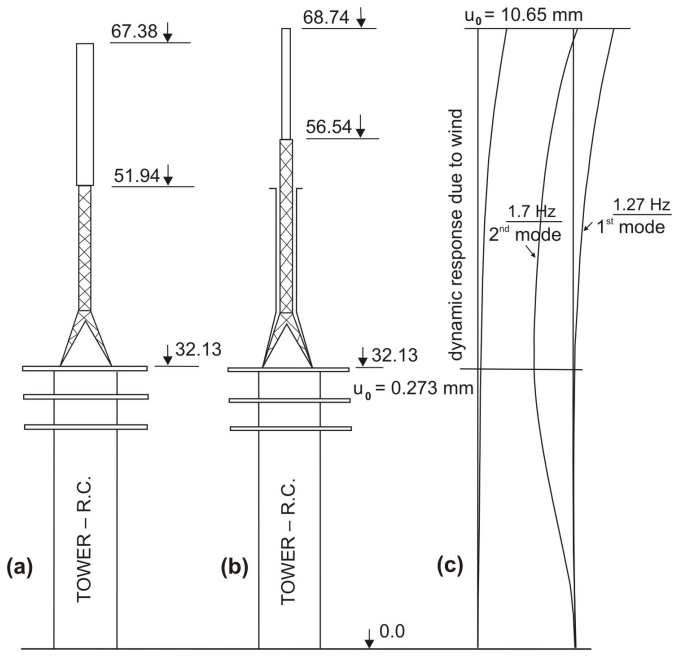

Figure 11: TV towers, their two lowest natural modes and amplitudes of wind induced vibrations

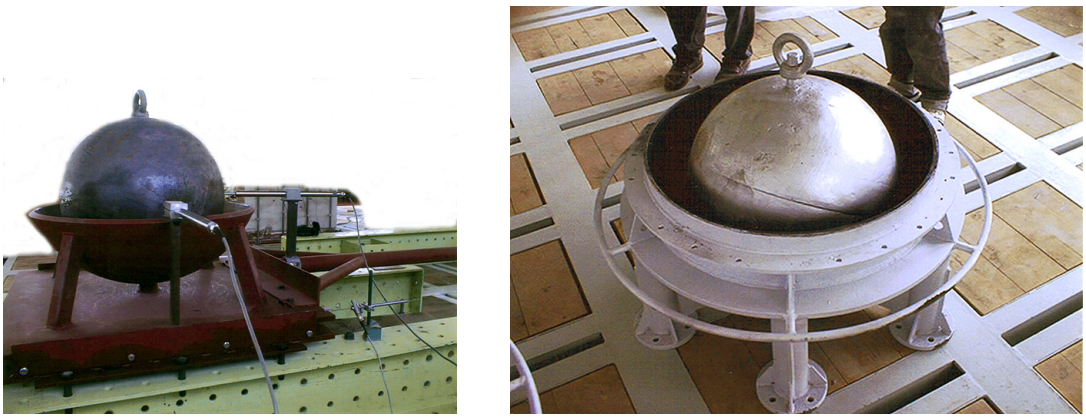

Figure 12: Ball absorber intended for a TV tower

Table 1: Ball absorber efficiency

	without absorber		with absorber		ratio with/without absorber	
Frequency $[Hz/s^{-1}]$	X	Y	X	Y	X	Y
0.90/5.65	0	0.0948	0	0.2031	-	2.14
1.27/7.98	19.064	3.279	0.271	0	0.0142	-
1.70/10.68	0	7.382	0	0.466	-	0.0632

$$X = f \cdot G_x(f)/\sigma_x^2 \; ; \quad Y = f \cdot G_y(f)/\sigma_y^2$$

frequencies using records of the long term measurements. For evaluation of absorber efficiency the following parameters has been introduced:

$$\varepsilon_x = \frac{f \cdot G_x(f)}{\sigma_x^2} \; ; \quad \varepsilon_y = \frac{f \cdot G_y(f)}{\sigma_y^2} \qquad (f = \omega/2\pi)$$

$G_x(f)$, or $G_y(f)$ – power spectral density of the tower top displacement in directions x, or y;

σ_x^2, or σ_y^2 – RMS of the tower top displacement in respective directions x, or y;

The scale of the response is presented in a form of a comparison of the values $\varepsilon_x, \varepsilon_y$ valid for the state without absorber (columns 2 and 3) and with absorber (columns 4 and 5), while columns 6 and 7 represent ratio of with/without absorber for respective directions. In particular, both columns 6 and 7 demonstrate high efficiency of the installed vibration absorber of ball type.

7 CONCLUSIONS

The vibration absorber of a ball type has been introduced. The basic Lagrangian analytical theory of non-linear behaviour has been done. Very wide numerical investigation reveals that the non-linear character of this device is an important factor influencing significantly its dynamic properties and practical efficiency. It turns out, that the non-linear character making the form of resonance curves dependent on the excitation amplitude leads to better efficiency in comparison with linear mechanism. For the same reason also chaotic component of the response can occur in certain frequency domains which increases significantly the efficiency of this device due to

higher energy loss. Laboratory tests of a ball vibration absorber with the dish without and with rubber coating have demonstrated several aspects of real operation of the damper . They have also proved the effectiveness of the damper and the influence of the rubber coating. With respect to laboratory tests and long-term in situ measurements can be concluded that the ball vibration absorber is a simple nearly maintenance free low cost device with very small vertical dimensions. For these properties it is very convenient for application especially in cases when broad band excitation of random character prevails and when very limited space is available.

The same experiments gave many results demonstrating various processes of stability loss and transition into various post-critical states under certain conditions. These phenomena remained without adequate theoretical explanation and without any assessment of influence onto damping properties. Therefore an intensive theoretical investigation should be provided. Detailed stability analysis is necessary to enable a reliable description of post-critical regimes, bifurcation points and corresponding transition effects involving the damping process. Also random parametric excitation and stochastic imperfection influence should be carefully studied.

ACKNOWLEDGEMENT

The kind support of the Czech Science Foundation project No. 103/09/0094, Grant Agency of the ASCR (projects No. IAA200710902, No. IAA200710805) and of the research plan AV OZ720710524 are gratefully acknowledged.

REFERENCES

[1] Pirner, M., Dissipation of kinetic energy of large-span bridges. *Acta Technica, CSAV*, **39**, 407-418, 1994.

[2] Pirner, M., Fischer, O., The development of a ball vibration absorber for the use on towers. *Jour.Int.Assoc.for Shell and Spatial Structures*, **41**(2), pp 91-99, 2000.

[3] Hamel, G., *Theoretische Mechanik*, Springer, Berlin, 1978.

[4] A. Tondl, A., *Quenching of Self-Excited Vibrations*. Academia, Prague, 1994.

[5] Xu Z., Cheung Y.K. (1994) Averaging method using generalized harmonic functions for strongly non-linear oscillators. *Journal of Sound and Vibration*, **174**(4), 563-576, 1994.

[6] Ren, Y., Beards, C.F., A new receptance-based perturbative multi-harmonic balance method for the calculation of the steady state response of non-linear systems. *Journal of Sound and Vibration*, **172**(5), 593-604, 1994.

[7] Náprstek, J., Fischer, C. (2009) Auto-parametric semi-trivial and post-critical response of a spherical pendulum damper *Computers and Structures*, **87**(19-20), 1204-1215, 2009.

[8] Náprstek, J., Pirner, M., Non-linear behaviour and dynamic stability of a vibration spherical absorber. In: *Proc. 15th ASCE Engineering Mechanics Division Conference* (A. Smyth et al. eds). Columbia Univ., New York, CD ROM, paper #150, 2002.